Redox Biology 71 (2024) 103090

Contents lists available at ScienceDirect

Redox Biology

journal homepage: www.elsevier.com/locate/redox

IL-4 activates ULK1/Atg9a/Rab9 in asthma, NLRP3 inflammasomes, and Golgi fragmentation by increasing autophagy flux and mitochondrial oxidative stress

Chang Xu [a,b,1], Yilan Song [a,b,1], Wanting Liu [a,b], Ruobai Liu [a,b], Qiaoyun Bai [a,b], Liangchang Li [a,b], Chongyang Wang [a,b,**], Guanghai Yan [a,b,*]

[a] Jilin Key Laboratory for Immune and Targeting Research on Common Allergic Diseases, Yanbian University, Yanji, 133002, PR China
[b] Department of Anatomy, Histology and Embryology, Yanbian University Medical College, Yanji, 133002, PR China

ARTICLE INFO

Keywords:
ULK1/Atg9a signaling pathway
Oxidative stress
Atg9a/Rab9 signaling pathway
Golgi apparatus fragmentation

ABSTRACT

During asthma, there is an intensification of pulmonary epithelial inflammation, mitochondrial oxidative stress, and Golgi apparatus fragmentation. However, the underlying mechanism remains largely unknown. Therefore, this study investigated the roles of ULK1, Atg9a, and Rab9 in epithelial inflammation, mitochondrial oxidative stress, and Golgi apparatus fragmentation. We found that ULK1 gene knockout reduced the infiltration of inflammatory cells, restored the imbalance of the Th1/Th2 ratio, and inhibited the formation of inflammatory bodies in the lung tissue of house dust mite-induced asthma mice. Moreover, we demonstrated that Atg9a interacted with ULK1 at S467. ULK1 phosphorylated Atg9a at S14. Treatment with ULK1 activator (LYN-1604) and ULK1 inhibitor (ULK-101) respectively promoted and inhibited inflammasome activation, indicating that the activation of inflammasome induced by house dust mite in asthma mice is dependent on ULK1. For validation of the *in vivo* results, we then used a lentivirus containing ULK1 wild type and ULK1-S467A genes to infect Beas-2b-ULK1-knockout cells and establish a stable cell line. The results suggest that the ULK1 S467 site is crucial for IL-4-induced inflammation and oxidative stress. Experimental verification confirmed that Atg9a was the superior signaling pathway of Rab9. Interestingly, we found for the first time that Rab9 played a very important role in inflammation-induced fragmentation of the Golgi apparatus. Inhibiting the activation of the ULK1/Atg9a/Rab9 signaling pathways can inhibit Golgi apparatus fragmentation and mitochondrial oxidative stress in asthma while reducing the production of NLRP3-mediated pulmonary epithelial inflammation.

1. Introduction

The prevalence of asthma is widespread, and the incidence rates of bronchial asthma are increasing annually [1]. In asthma patients, Th1 cell function decreases while Th2 cell function abnormally increases. This results in the disrupted production of various inflammatory factors, including insufficient generation of interferon-γ (IFN-γ), and increased secretion of interleukin-4 (IL-4) and interleukin-5 (IL-5) [2]. There is a relationship among the Th2 cytokine IL-4, the interleukin-13 (IL-13), the production of IgE, the eosinophil infiltration of the lungs, and the airway hyperresponsiveness [3].

Unc-51-like autophagy activating kinase 1 (ULK1) and autophagy-related 9a (Atg9a) play essential roles in autophagy [4]. They are also implicated in inflammatory diseases. For instance, in neuroinflammation, p38 MAPK promotes the inflammatory response of microglia cells through phosphorylation of ULK1 [5]. Inflammatory diseases and tumors involve the formation of complexes on Atg9a vesicles during ULK1 activation, which plays a crucial role in regulating innate immune signaling and tumor development [6]. Additionally, studies have revealed that the ULK1-NLRP3 (nucleotide-binding

* Corresponding author. Department of Anatomy, Histology and Embryology, Yanbian University Medical College, No. 977, Gongyuan Road, Yanji 133002, PR China.,
** Corresponding author. Department of Anatomy, Histology and Embryology, Yanbian University Medical College, No. 977, Gongyuan Road, Yanji, 133002, PR China.
E-mail addresses: m18804331583@163.com (C. Wang), ghyan2015@sina.com, ghyan@ybu.edu.cn (G. Yan).
[1] These authors contributed equally to this work.

https://doi.org/10.1016/j.redox.2024.103090
Received 18 January 2024; Received in revised form 8 February 2024; Accepted 14 February 2024
Available online 15 February 2024

oligomeric domain-like receptor protein 3)-pyroptosis pathway can lower the level of pyroptosis in acute liver failure [7]. Moreover, Atg9a ubiquitination has been found to play a critical role in oxidative stress-induced autophagy, endocytic transport, and innate immunity [8]. However, the involvement of ULK1 and Atg9a in the pathogenesis of asthma has yet to be examined.

Rab9 GTPase (Rab9), a small GTPase of the Ras family, serves as an advanced endosomal protein marker. It is shown that Rab9 expression is associated with enhanced mitochondrial localization [9]. A variety of differentially expressed in normal and neoplastic cells (DENN) domains directly interact with members of the Rab family of small GTPases, suggesting that DENN domain proteins act as generalized regulators of Rab function [10]. DENND1B mutations have been linked to the development of childhood asthma and other immune diseases [11]. Consequently, it can be inferred that the small GTPase family of Rab is implicated in the pathogenesis of asthma. Rab9 plays a crucial role in the transport between late endosomes and the trans-Golgi network [12]. The formation of Golgi stacks is essential for the proper functioning of the Golgi apparatus. Golgi protein subfamily A member 2 and Golgi reassembly stacking protein of 65 KD (GRASP65) are necessary for Golgi band formation. When cells are under oxidative stress, fragmentation of the Golgi apparatus increases the production of antioxidant proteins and activates the NLRP3-mediated inflammatory response [13]. Therefore, we speculate that the Golgi apparatus may undergo corresponding changes during the onset of asthma, with Rab9 playing a crucial role.

Asthma can lead to energy stress, which can cause mitochondrial damage and result in lung cell death [14]. Reactive oxygen species (ROS) can affect mitochondrial membrane potential, trigger the release of Ca^{2+} and cytochrome C, induce cytotoxicity, disrupt mitochondrial DNA (mtDNA) transcription and translation, and hinder the synthesis of mtDNA coding proteins [15,16]. It is shown that oxidative stress can activate the ULK1 pathway [17]. Wang et al. reported that the ubiquitination of Atg9a played a crucial role in oxidative stress, endocytic transport, and innate immunity [18]. Consequently, this suggests the involvement of ULK1 and Atg9a signaling pathways in oxidative stress responses.

Currently, it is known that NLRP3 inflammasomes are activated during the onset of asthma, and inhibiting their activation can prevent asthma [19]. Thus, developing effective inhibitors for NLRP3 inflammasomes is of utmost importance. Research has found that Beclin 2 interacts with inflammasome sensors through ULK1 and Atg9a, and it recruits inflammasome sensors on Atg9a vesicles [20]. ULK1 and Atg9a proteins can potentially regulate the activation of inflammasomes and inflammation, making them potential therapeutic targets for the treatment of infectious and inflammatory diseases. Nevertheless, the mechanism by which ULK1 and Atg9a affect NLRP3 inflammasomes in asthma remains to be studied.

Several studies [21,22] have established a link between inflammation and mitochondrial oxidative stress in the development of asthma. However, the exact mechanisms involved in this interaction remain unknown. The main focus of this study is to explore the potential involvement of the ULK1/Atg9a signaling pathways in the occurrence of epithelial inflammation and ROS during asthma onset. Our findings may provide evidence for developing novel therapeutic targets for asthma treatment.

2. Materials and methods

2.1. Study animals

The female wild type (WT) (n = 35) and ULK1$^{-/-}$ mice (n = 25) (average body weight: 20 g, approximately 6–8 weeks) were purchased from the Laboratory Animal Management Center of Yanbian University (certificate number: SYXK (Ji) 2020 0010). The experimental procedures were strictly carried out following the requirements of the "Regulations on the Management of Experimental Animals". This study was approved by the Ethics Committee of Yanbian University.

2.2. Animal grouping and treatment

WT mice were divided into WT, WT + PBS, WT + HDM (house dust mite), WT + HDM + LYN-1604 hydrochloride, WT + HDM + ULK-101, WT + HDM + siControl, and WT + HDM + siRab9, with 5 mice in each group. ULK1$^{-/-}$ mice were divided into ULK1$^{-/-}$, ULK1$^{-/-}$ + PBS, ULK1$^{-/-}$ + HDM, ULK1$^{-/-}$ + HDM + LYN-1604 hydrochloride, and ULK1$^{-/-}$ + HDM + ULK-101, with 5 mice in each group. Except for the WT, WT + PBS, ULK1$^{-/-}$ and ULK1$^{-/-}$ + PBS, mice in other groups received intranasal (i.n.) drops of 50 μg HDM (Greer Laboratories, Lenoir, NC, USA, XPB46D3A4) on days 0, 7, and 14. Mice in the model and treatment groups were challenged daily with 50 μg HDM i.n. instilled on days 21–27. The mice in the WT + PBS and ULK1$^{-/-}$ + PBS groups received PBS as a control. For signal pathway analysis, LYN-1604 hydrochloride (MCE, USA, HY-101923A) and ULK-101 (MCE, USA, HY-114490) were dissolved in DMSO and injected intraperitoneally at a dose of 20 mg/kg on days 17–27. For mice in ULK1-WT + HDM + siControl and ULK1-WT + HDM + siRab9 groups, nasal drips of siControl and siRab9 (Ribobio, China) were administered every three days.

2.3. Cell culture and treatment

Cell lines 16HBE and Beas-2b were cultured in DMEM medium supplemented with 10% fetal bovine serum and 100 U/mL penicillin/streptomycin. The cells were incubated in a 37 °C incubator with 5% CO_2 until they reached 80% confluency. After MitoQ (FOCUS Bioolecus, USA) pretreatment for 1 h, IL-4 was added to induce inflammation. Beas-2b cells were then stimulated with IL-4 (MCE, USA, HY-P7042) at a concentration of 100 ng/L and incubated at 37 °C for 0 h, 6 h, 12 h, and 24 h. For transfection, Beas-2b cells were seeded onto a 6-well plate at a density of 2×10^5 cells per well and transfected with siControl, siULK1, siAtg9a, and siRab9 (Ribobio, Guangzhou, China) using Lipofectamine3000 (Thermo Fisher Scientific, USA, L300075). After transfection for 6 h, fresh DMEM was added and cells were further cultured for 48 h. Beas-2b-ULK1-knockout (KO) cells (Cyagen, Guangzhou, China) were infected with Lentivirus containing ULK1-WT and ULK1-S467A genes to establish stable cell lines.

2.4. Western blotting

Proteins extracted from lung tissue or cells were quantified using the BCA protein detection reagent (Thermo Fisher Scientific, USA, 23225). Each protein sample was separated by SDS-PAGE or Phos-tag SDS-PAGE and transferred to the membranes, which were then blocked with 5% skimmed milk for 1 h. Following this, incubation with primary antibodies against ULK1 (CST, USA, # 8054), Atg9a (CST, USA, # 13509), Rab9 (CST, USA, # 5133), NLRP3 (CST, USA, # 15101), caspase-1 (CST, USA, # 24232), IL-1β (CST, USA, # 31202), GRASP65 (Thermo Fisher Scientific, USA, PA3-910), p-Ser/Thr (CST, USA, # 9631S), LC3A/B (CST, USA, # 4108S), and β-actin (CST, USA, # 3700) was performed overnight at 4 °C. The incubation with the secondary antibody was conducted at room temperature for 2 h. After color development, the protein bands were analyzed with Image J software (version 1.8.0, National Institutes of Health).

2.5. In vitro ULK1 kinase assay

Beas-2b cell lysate or immunoprecipitated GFP-ULK1, along with purified His ATG9N-HA and 100 μM ATP in ULK1 kinase buffer (containing 25 mM HEPES, pH 7.4, 50 mM NaCl, 5 mM $MgCl_2$, and 1 mM DTT), were incubated at 30 °C for 30 min. The reaction was stopped by adding a sample buffer, followed by analysis using Western blotting.

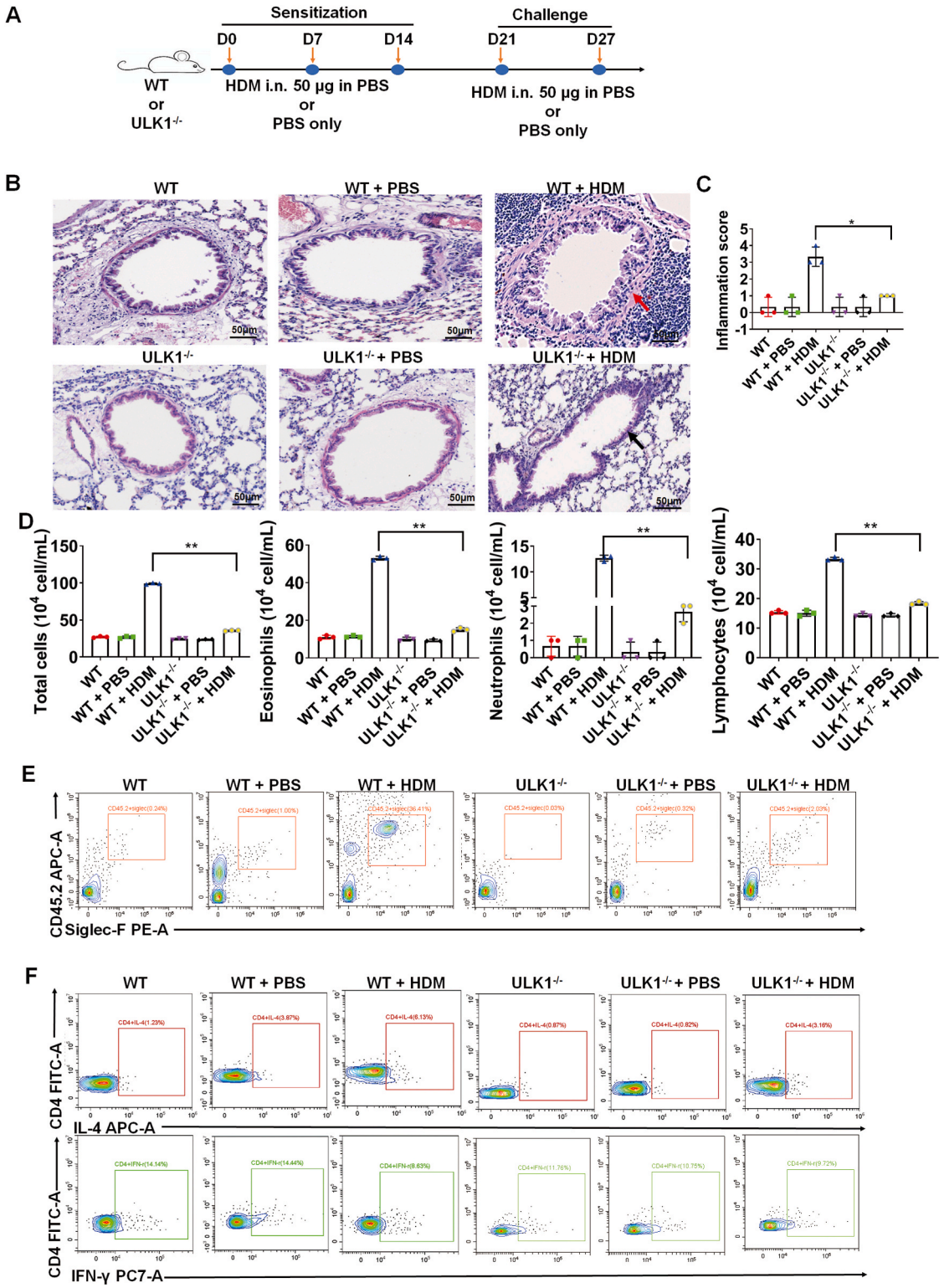

Fig. 1. Effect of ULK1 on HDM-induced inflammatory response in asthma.
A. Schematic diagram of asthma modeling in ULK1-WT and ULK1$^{-/-}$ mice. The mice in the WT + HDM group and ULK1$^{-/-}$ + HDM group were given 50 μg HDM i.n. on days 0, 7, and 14, and injected with 50 μg HDM every day on days 21–27. WT + PBS group and ULK1 $^{-/-}$ + PBS group were used as control. **B.** H&E staining images of lung tissues (scale: 50 μm). The red arrow indicates the thickened trachea, with a narrowing of the bronchial cavity and a substantial infiltration of inflammatory cells surrounding the bronchus. The black arrow indicates less thickened trachea and a minor infiltration of inflammatory cells around the bronchus. **C.** The inflammation score of H&E staining images in each group was compared. **D.** Cell counts after Diff-Quik staining of BALF. **E.** Representative flow cytometry results on eosinophils in BALF. Eosinophils were stained with APC-conjugated CD45.2 and PE-conjugated siglec-F antibodies. **F.** Representative flow cytometry results on CD4^{+}IL-4- and CD4^{+}IFN-γ-positive cells in BALF. *$p < 0.05$, **$p < 0.01$. (For interpretation of the references to color in this figure legend, the reader is referred to the Web version of this article.)

2.6. H&E staining

The left lung tissues were fixed, embedded, and cut into 5 μm sections. H&E staining was performed according to routine procedures. The inflammation scores were calculated as previously described [23,24].

2.7. Diff-Quik staining

After modeling, the mice were perfused with PBS solution containing BSA to collect tracheal, bronchial, and whole lung lavage, i.e. BALF. Cells from 1 ml of lavage were smeared, and rapid staining was performed with Diff-Quik (Solarbio, China, G1540). The number of total cells, eosinophils, macrophages, lymphocytes, and neutrophils was counted.

2.8. Flow cytometry analysis of eosinophils, IL-4 and IFN-γ

BALF were fixed at room temperature in the dark for 30 min and then incubated with fluorescent-labeled eosinophil antibodies of PerCP-Cyanine5.5-CD11c (Thermo Fisher Scientific, USA, 45-0114-80), APC-CD45.2 (Thermo Fisher Scientific, USA, 17-0454-82), and PE-siglec-F (Thermo Fisher Scientific, USA, 12-1702-82). After that, fluorescent-labeled $CD4^+$ cell antibodies FITC-$CD4^+$ (Thermo Fisher Scientific, USA, 11-0049-80) and PE-$CD8^+$ (Thermo Fisher Scientific, USA, MA5-44117) were added and incubated at room temperature in the dark for 30 min. After permeation and washing, the cells were incubated in the dark with fluorescent-labeled cytokine antibodies APC-IL-4 (Thermo Fisher Scientific, USA, 17-7041-82) and PE-Cy7-IFN- γ (Thermo Fisher Scientific, USA, 25-7311-82), at room temperature for 30 min. Following washing, cells were analyzed on CytoFLEX (Beckmann).

2.9. Co-immunoprecipitation (CO-IP)

Beas-2b was transfected with plasmids of ULK1 pcDNA6 Flag, Atg9a pcDNA6 Myc, and various fragments of ULK1 using Lipofectamine ™ 3000. After overnight transfection, cell samples were collected and lysed. CO-IP was performed using the Anti-FLAG ® M2 magnetic beads. The eluted proteins were detected with Western blotting.

2.10. Immunofluorescence

After antigen repair, the lung tissue sections or cell slides were fixed for 30 min and permeabilized with TritonX-100 for 30 min. After blocking with 3% BSA, the samples were incubated with primary antibodies of anti-ULK1, anti-Atg9a, anti-Rab9, anti-TOM20 (CST, USA, #42406), and anti-DNA (PROGEN, Germany, AC-30-10), overnight at 4 °C. The incubation with the secondary antibody was performed at room temperature in the dark for 1 h. Finally, the samples were observed under the Cytation5 (BioTek, USA). The average fluorescence intensity was detected by the BioTek Cytation 5 cell imaging multifunctional microplate detection system to semi-quantitatively analyze the protein expression.

2.11. Golgi staining

To perform Golgi staining, first, the cell culture medium was removed and the cells on the cover glass were washed with an appropriate amount of solution (HBSS with Ca2+ & Mg^{2+}; Beyotime, C0219). Then, the washing solution was discarded and Golgi Tracker Red (Beyotime, C1043) was added to the cells and incubated at 4 °C for 30 min. The cells were washed with pre-cooled cell culture medium in an ice bath approximately three times, followed by incubation with fresh culture medium at 37 °C for 30 min. Subsequently, the cells were washed again with fresh culture medium and observed using a fluorescence microscope or laser confocal microscope. At this stage, the Golgi apparatus exhibited bright, strong fluorescence staining, whereas other membrane systems within the cell showed relatively weak fluorescence staining.

2.12. Mito-SOX, JC-1, and 3-AM staining

The cells were washed 3 times with HBSS solution and then incubated with Mito-SOX (M36008, Invitrogen, USA), JC-1 (C2006, Beyotime, China), or Fluo 3-AM working solution (F8840, Solarbio, Beijing) at 37 °C for 10 min. The cells were observed under a laser confocal microscope after DAPI staining.

2.13. Transmission electron microscope

Lung tissue or cells measuring 1 mm × 1 mm (half the size of mung beans) were collected, fixed with 4% glutaraldehyde for 3 h, and then placed in PBS at 4 °C. The collected tissue or cells were pre-embedded in 1% agar and fixed in 0.1 M phosphate buffer (pH 7.4) with 1% osmic acid for 2 h at room temperature in the dark. The tissue or cells underwent gradual ethanol dehydration at room temperature, followed by gradual acetone permeation embedding in resin. The embedding plate was placed in a 60 °C oven for polymerization for 48 h. Finally, the tissue or cells were observed under a transmission electron microscope, and images were captured for analysis.

2.14. Construction of protein-protein interaction network

We utilized the STRING database (https://cn.string-db.org/) to construct the protein-protein interaction network. The ULK1 and Atg9a were filtered and input into MultiProt. The auto-detect feature was then used to generate the protein interaction network. Then, the species of *Homo sapiens* and *Mus musculus* were selected.

2.15. Statistical analysis

The data were analyzed using the statistical software SPSS version 20.0. The results from three independent experiments are presented as the means ± standard error of the mean. All data were of normal distribution, as determined by the Shapiro-Wilk test. One-way ANOVA and Duncan's multiple-range tests were conducted to determine statistical significance. A significance level of $p < 0.05$ was used to indicate a statistically significant difference.

3. Results

3.1. HDM-induced inflammatory response in asthma is relieved after ULK1 knockout

The protocol for establishing HDM-induced asthma in WT and $ULK1^{-/-}$ mice is presented in Fig. 1A. H&E staining showed that in the WT + HDM group, the trachea was thickened, with a narrowing of the bronchial cavity and a substantial infiltration of inflammatory cells surrounding the bronchus (Fig. 1B). In contrast, the $ULK1^{-/-}$ + HDM group showed less pronounced tracheal thickening and only a minor infiltration of inflammatory cells around the bronchus (Fig. 1B). Statistically, the inflammation score was significantly reduced in the $ULK1^{-/-}$ + HDM group than in the WT + HDM group (Fig. 1C). As shown in Fig. 1D, the $ULK1^{-/-}$ + HDM group demonstrated a significantly lower total number of cells, eosinophils, neutrophils, and lymphocytes in BALF when compared to the WT + HDM group. Flow cytometry was used to detect eosinophils in BALF, which showed that the knockout of ULK1 could effectively inhibit the production of eosinophils stimulated by HDM (Fig. 1E).

The hallmarks of allergic asthma, particularly the progressive worsening, are directly associated with immunological memory T cells, specifically $CD4^+$ Th2 cells [2]. Type 2 immunity, which results from the upregulation of the $CD4^+$ T cell subtype Th2 and its cytokine IL-4, plays

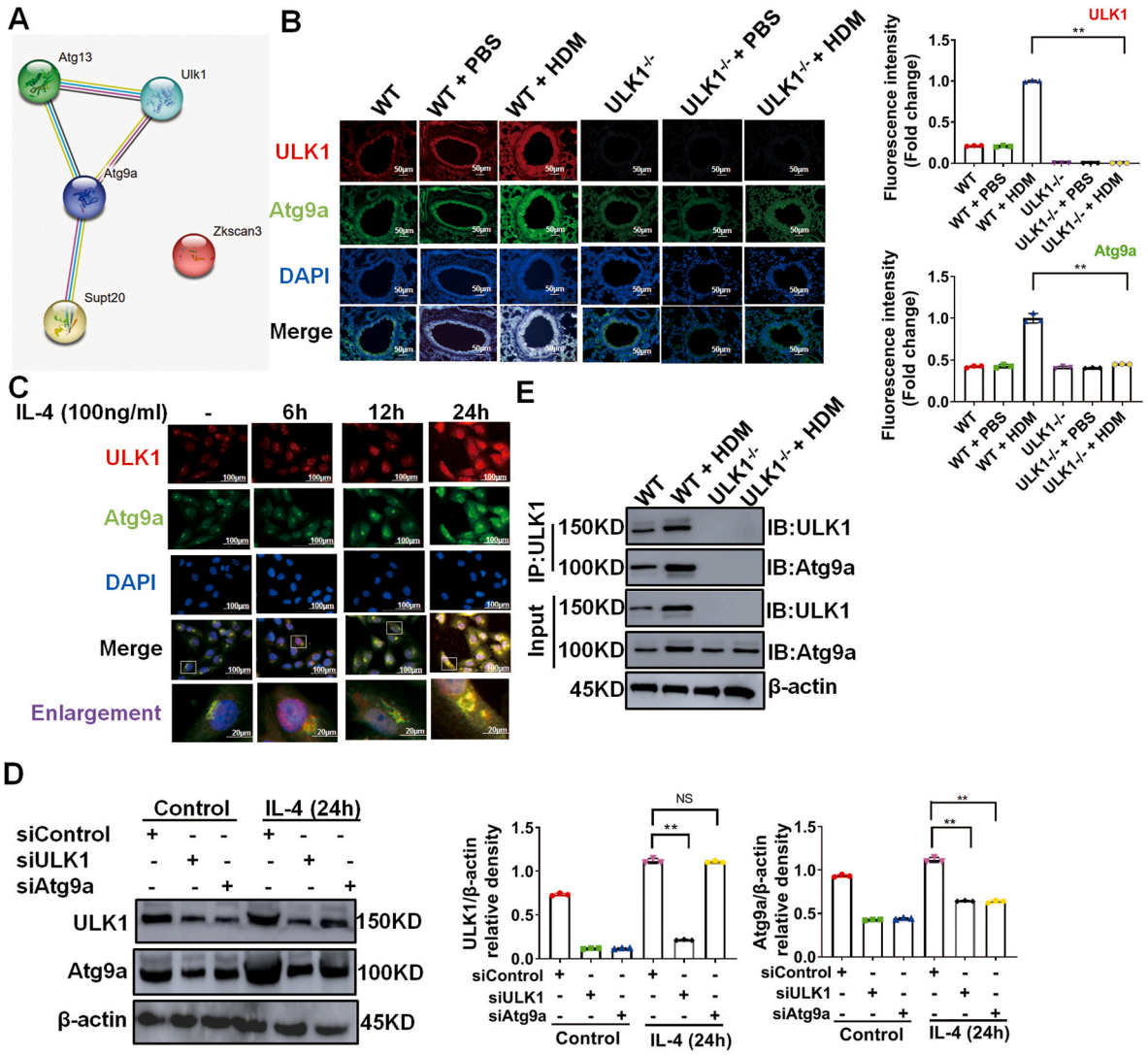

Fig. 2. ULK1/Atg9a signaling pathway is involved in asthma.
A. The protein-protein interaction network through the STRING database. **B.** Immunofluorescence was used to measure the expression of ULK1 and Atg9a in mouse lung tissue (scale: 50 μm). **C.** Immunofluorescence was used to measure the expression of ULK1 and Atg9a in Beas-2b cells (scale: 100 μm). **D.** Western blotting was used to measure the expression of ULK1 and Atg9a in Beas-2b after silencing ULK1 or Atg9a and IL-4 stimulation. **E.** CO-IP results detected by Western blotting. $^{**}p < 0.01$. The original full gel blots are presented in the supplementary material.

a critical role in the pathogenesis of allergic asthma. We found by flow cytometry (Fig. 1F) that treatment with HDM led to an increase in IL-4 levels, indicating Th2 response, and a reduction in IFN-γ levels, indicating Th1 response. Compared to the WT + HDM group, the ULK1$^{-/-}$ + HDM group exhibited decreased proportions of IL-4 positive cells in mouse BALF and elevated proportions of IFN-γ positive cells. These results suggest that the knockout of ULK1 reduces the inflammatory response in HDM-induced asthma.

3.2. *ULK1/Atg9a signaling pathway is involved in the occurrence of asthma*

The STRING database was used to analyze the interaction between multiple proteins, especially ULK1 and Atg9a. A protein-protein interaction network was generated (Fig. 2A). After importing species data for *Homo sapiens* and *Mus musculus*, it was observed that only ULK1 and Atg9a could interact with each other. There is currently no experimental evidence to support the co-expression of ULK1 and Atg9a in certain homologous species. To confirm this theory, we isolated proteins from Beas-2b cells, 16HBE cells, and mouse lung tissue. Western blotting confirmed the expression of ULK1 and Atg9a in both Beas-2b and 16HBE cells (Supplementary Fig. S1). Additionally, the expression of ULK1 and Atg9a was stronger in Beas-2b cells compared to 16HBE cells. As a result, Beas-2b cells were used for the subsequent *in vitro* experiments.

Immunofluorescence staining of ULK1 and Atg9a in lung tissues showed that their levels were significantly lower in the ULK1$^{-/-}$ + HDM group compared to the WT + HDM group (Fig. 2B). Similarly, in Beas-2b cells, the expression of ULK1 and Atg9a significantly increased after 24 h of IL-4 stimulation (Fig. 2C). Furthermore, ULK1 and Atg9a were both present in the perinuclear cytoplasm. Then, ULK1 and Atg9a were silenced in Beas-2b cells after 24 h of IL-4 stimulation. The expression of ULK1 and Atg9a was examined using Western blotting. The siULK1+IL-4 group showed a significant decrease in both Atg9a and ULK1 expression compared to the siControl + IL-4 group (Fig. 2D). However, in the siAtg9a + IL-4 group, only the expression of Atg9a decreased. This suggests that ULK1 may be upstream of Atg9a. CO-IP demonstrated that there was an interaction between ULK1 and Atg9a in mouse lung tissue and this interaction was enhanced by HDM stimulation (Fig. 2E). Therefore, the ULK1/Atg9a signaling pathway may be involved in the development of asthma.

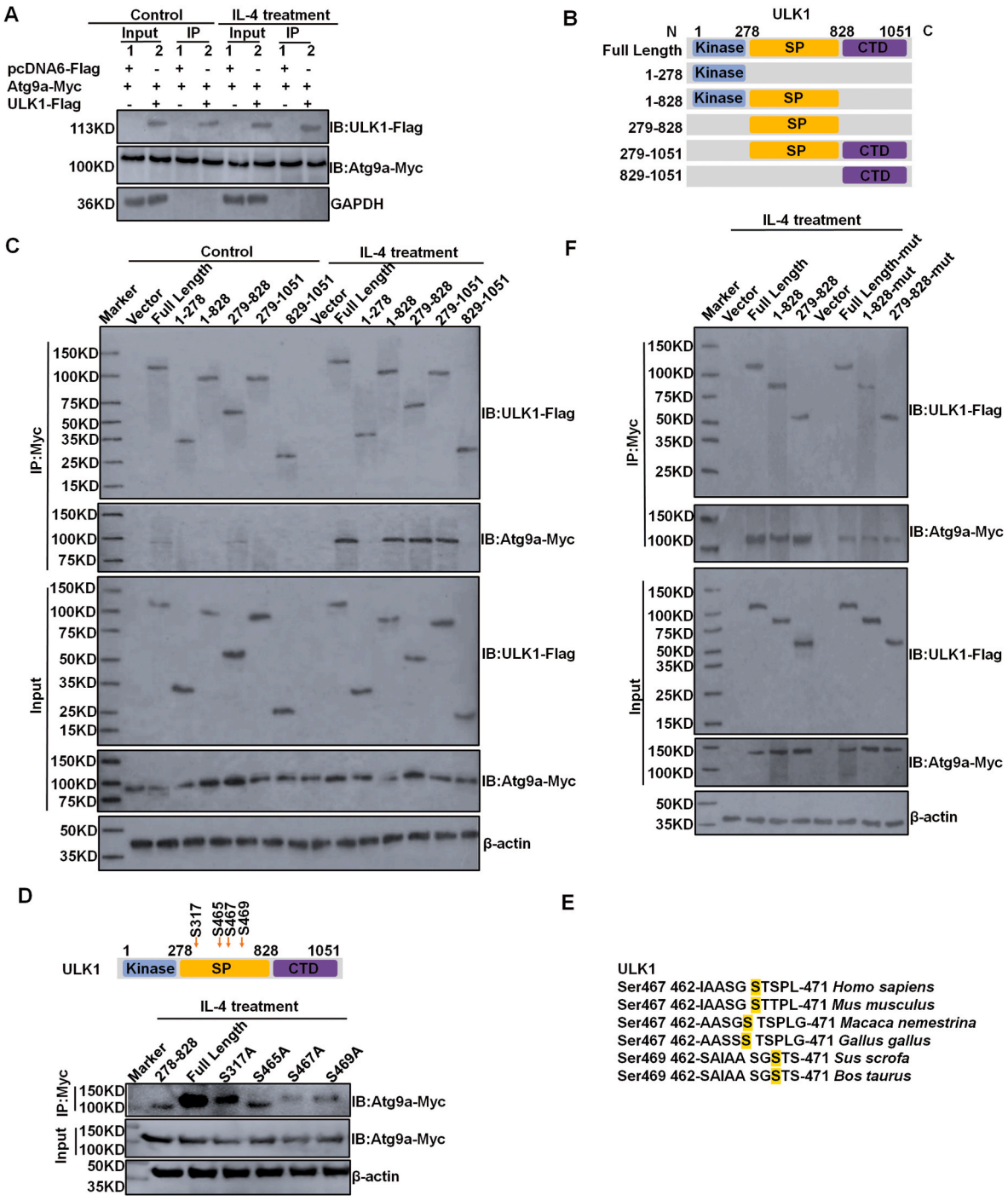

Fig. 3. ULK1 S467 is a crucial site involved in the interaction with Atg9a.
Beas-2b was transfected with plasmids of ULK1 pcDNA6 Flag, Atg9a pcDNA6 Myc, and ULK1 fragments. **A.** CO-IP detection of ULK1 and Atg9a in Beas-2b cells treated with IL-4. **B.** Composition of ULK1. **C.** The region of interaction between ULK1 and Atg9a after IL-4 treatment. **D.** The potential sites on fragments 279–828 of ULK1 for interactions with Atg9a. **E.** Ser467 in ULK1 exhibits evolutionary conservation. **F.** ULK1 S467 mutation and the binding ability of ULK1 to Atg9a was detected by CO-IP. The original full gel blots are presented in the supplementary material.

3.3. ULK1 S467 is a crucial site involved in the interaction with Atg9a

The Co-IP results demonstrated the interaction between ULK1 and Atg9a in IL-4-treated Beas-2B cells (Fig. 3A). ULK1 consists of three parts: the kinase domain (1–278), the serine proline-rich spacer (279–828), and the C-terminal domain (829–1051) (Fig. 3B). Further Co-IP detection revealed that following IL-4 treatment, the segments 1–828, 279–828, and 279–1050 of ULK1 interacted with Atg9a (Fig. 3C). The results suggest that the spacer region plays a crucial role in regulating the interaction between ULK1 and Atg9a.

Segments 279–828 of ULK1 were found to contain potential sites that interacted with Atg9a (Fig. 3D). Through Co-IP detection, we determined that S467 was the specific site we were interested in. Ser467 of ULK1 was found to be evolutionally conserved (Fig. 3E). To investigate the binding capacity of ULK1 to Atg9a, we introduced a mutation in ULK1 S467. This mutation significantly reduced the binding capacity between Atg9a and ULK1 (Fig. 3F). Based on these findings, it is evident that ULK1 S467 is a crucial site involved in the interaction with Atg9a.

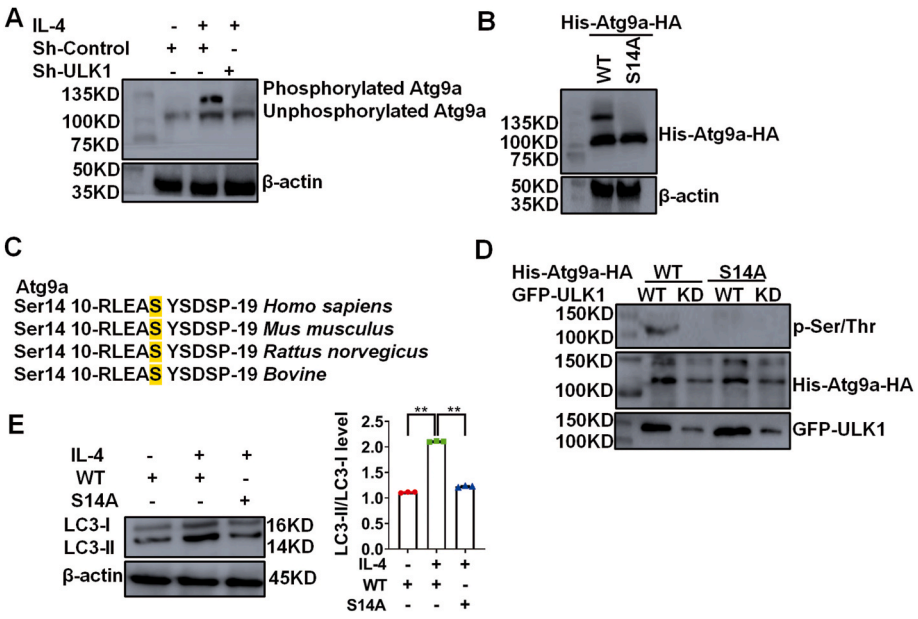

Fig. 4. ULK1 directly phosphorylates Atg9a at S14.
A. Phosphorylation of Atg9a was analyzed using Phos-tag SDS-PAGE. **B.** Analysis of the phosphorylation sites of Atg9a using Phos-tag SDS-PAGE. **C.** Ser14 in Atg9a exhibited evolutionary conservatism. **D.** In vitro ULK1 kinase assay. WT, wild type; KD, kinase-dead. **E.** Western blotting was used to measure the expression of LC3I and LC3II in Beas-2b-Atg9a KO cells stimulated by IL-4. **F.** The relative level of LC3 II/I. **p < 0.01. The original full gel blots are presented in the supplementary material.

3.4. ULK1 directly phosphorylates Atg9a at S14

Phos-tag SDS-PAGE was utilized to analyze Atg9a phosphorylation in Beas-2b cells upon IL-4 stimulation (Fig. 4A). A band at approximately 100 kDa in all three lanes represented the unphosphorylated form of Atg9a. In the IL-4+sh Control group, the anti-Atg9a antibodies detected a higher molecular weight, indicating a singly phosphorylated form of Atg9a. The role of ULK1 in coordinating Atg9a phosphorylation and its involvement in the sorting of membrane vesicle transport in cellular autophagy has been demonstrated [25]. Furthermore, sequence alignment revealed that the S14 residue of Atg9a was situated within the conserved phosphorylation motif of the ULK1 kinase [25]. Subsequently, Phos-tag SDS-PAGE was employed to analyze the particular phosphorylation sites of Atg9a in Beas-2b cells (Fig. 4B). Two bands of anti-Atg9a antibody were observed in the Atg9a-WT group. The upper band in the Atg9a-S14A group was absent, signifying the presence of S14 as a phosphorylation site in Atg9a. Ser14 of Atg9a was determined to be evolutionarily conserved (Fig. 4C).

The *in vitro* kinase assay demonstrated that WT-ULK1, as opposed to the kinase-dead ULK1, directly phosphorylated purified Atg9a. It was observed that only the S14A mutation abolished phosphorylation signals, suggesting that S14 is a specific phosphorylation site for ULK1 kinase (Fig. 4D). Western blotting revealed that the Atg9a S14 mutation significantly reduced the level of LC3-II/LC3-I under IL-4 stimulation, suggesting that Atg9a S14 is a crucial site for autophagy (Fig. 4E). The aforementioned findings suggest that under IL-4 stimulation, ULK1 phosphorylates Atg9a directly at S14, which is a pivotal site for regulating autophagy.

3.5. HDM activates NLRP3 through the ULK1/Atg9a signaling pathway

Western blotting found that the protein levels of NLRP3, caspase-1, and IL-1β in lung tissue decreased in the ULK1−/− + HDM group, in contrast to the WT + HDM group (Fig. 5A). LYN-1604, a small chemical compound, has shown great potential as a ULK1 agonist [25]. In this study, WT and ULK1$^{-/-}$ mice were administered LYN-1604 from days 17–23 (Fig. 5B). On days 21–23, the animals were stimulated with HDM or PBS. Western blotting analysis revealed that in WT mice, the LYN-1604 + HDM group exhibited increased expression levels of ULK1 and p-Atg9a (Fig. 5C), as well as elevated levels of NLRP3, caspase-1, and IL-1β (Fig. 5D), compared to the HDM group. However, there were decreased levels of NLRP3, caspase-1, and IL-1β in the LYN-1604 + HDM group of ULK1$^{-/-}$ mice in comparison to the LYN-1604 + HDM group of WT mice (Fig. 5D). Consequently, the study revealed that administering a ULK1 agonist to asthmatic mice induced by HDM may potentially induce the production of inflammasomes.

In response to various stimuli, ULK-101 inhibits both the induction and the flux of autophagy [26]. Here, we also verified the effect of ULK1 on inflammasomes by using ULK-101. WT and ULK1$^{-/-}$ mice were administered ULK-101 from days 17–23, and HDM or PBS stimulation was used from days 21–23 (Fig. 5E). Western blot analysis showed that in WT mice, the ULK-101 + HDM group exhibited lower levels of ULK1 and p-Atg9a expression (Fig. 5F), and reduced levels of NLRP3, caspase-1, and IL-1β (Fig. 5G) compared to the HDM group. NLRP3 expression decreased when comparing WT mice and ULK1−/− mice in the ULK-101 + HDM groups. It is worth noting that the addition of ULK1 inhibitors in asthmatic mice triggered by HDM can prevent the production of inflammasomes.

3.6. IL-4-induced NLRP3 activation depends on the ULK1/Atg9a signaling pathway

Beas-2b cells were stimulated with IL-4 for 0 h, 6 h, 12 h, and 24 h, respectively. Western blotting demonstrated significantly increased expression of NLRP3, caspase-1, and IL-1β at 24 h (Fig. 6A). Moreover, compared with the siControl + IL-4 group, the siULK1+IL-4 group exhibited decreased levels of NLRP3, caspase-1, and IL-1β (Fig. 6B). The intracellular calcium ion concentration can increase due to the activation of NLRP3 [27].

Fluo 3-AM staining was used to determine the Ca^{2+} content in Beas-2b cells induced by IL-4 (Fig. 6C). The results indicated that intracellular calcium ions predominantly accumulated in the cytoplasm of Beas-2b cells. The concentration of intracellular calcium ions progressively increased, peaking at 24 h. Following IL-4 stimulation for 24 h, both

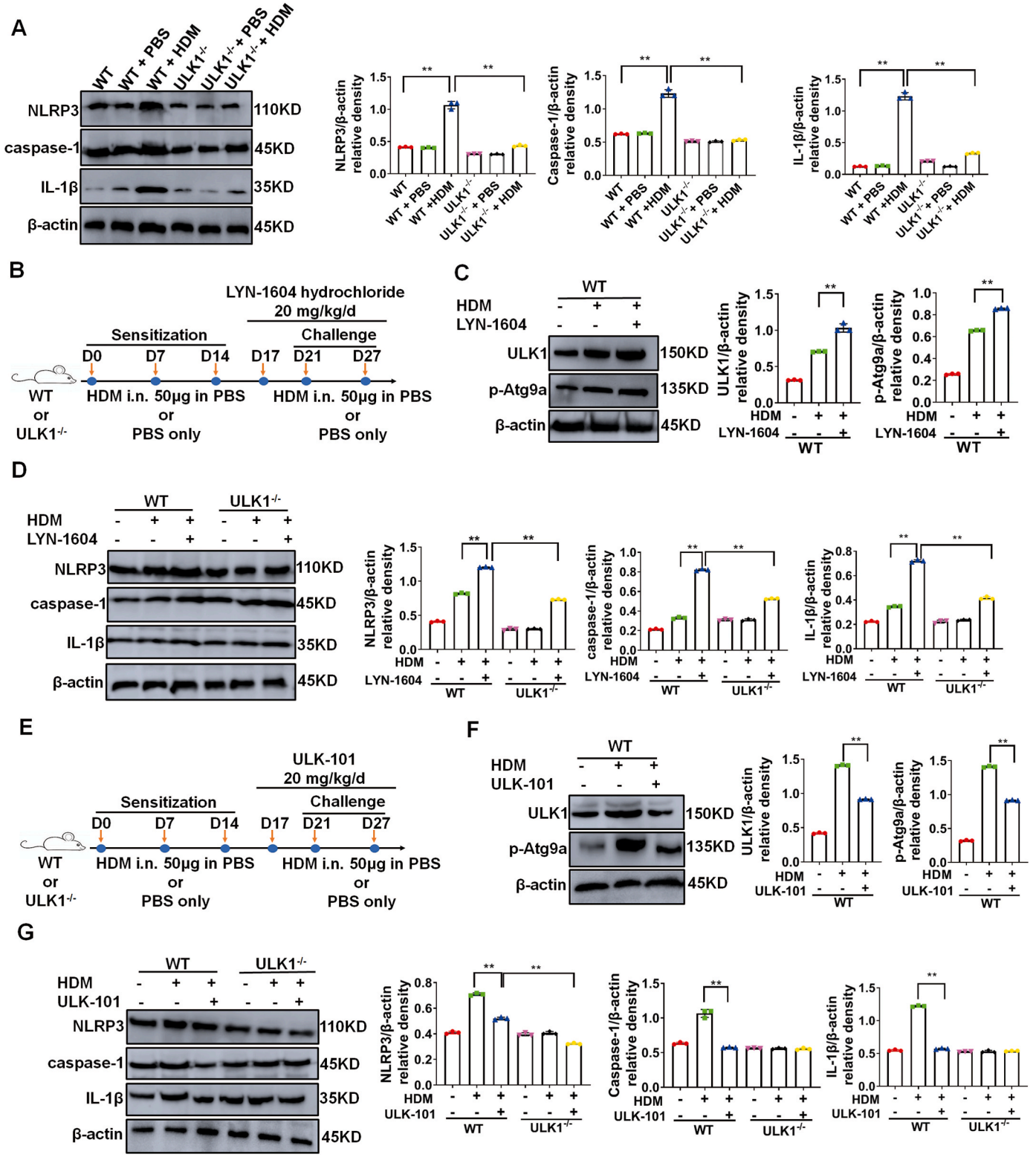

Fig. 5. HDM activates NLRP3 through the ULK1/Atg9a signaling pathway.
A. Western blotting detection of NLRP3, caspase-1, and IL-1β in lung tissues. **B.** Schematic diagram of LYN-1604 administration in ULK1-WT and ULK1$^{-/-}$ mice. **C.** Western blotting analysis of the expression of ULK1, p-Atg9a, and Atg9a. **D.** Western blotting analysis of NLRP3, caspase-1, and IL-1β. **E.** Schematic diagram of ULK-101 administration in ULK1-WT and ULK1$^{-/-}$ mice. **F.** Western blotting analysis of ULK1, p-Atg9a, and Atg9a expression. **G.** Western blotting analysis of NLRP3, caspase-1, and IL-1β expression. $^{**}p < 0.01$. The original full gel blots are presented in the supplementary material.

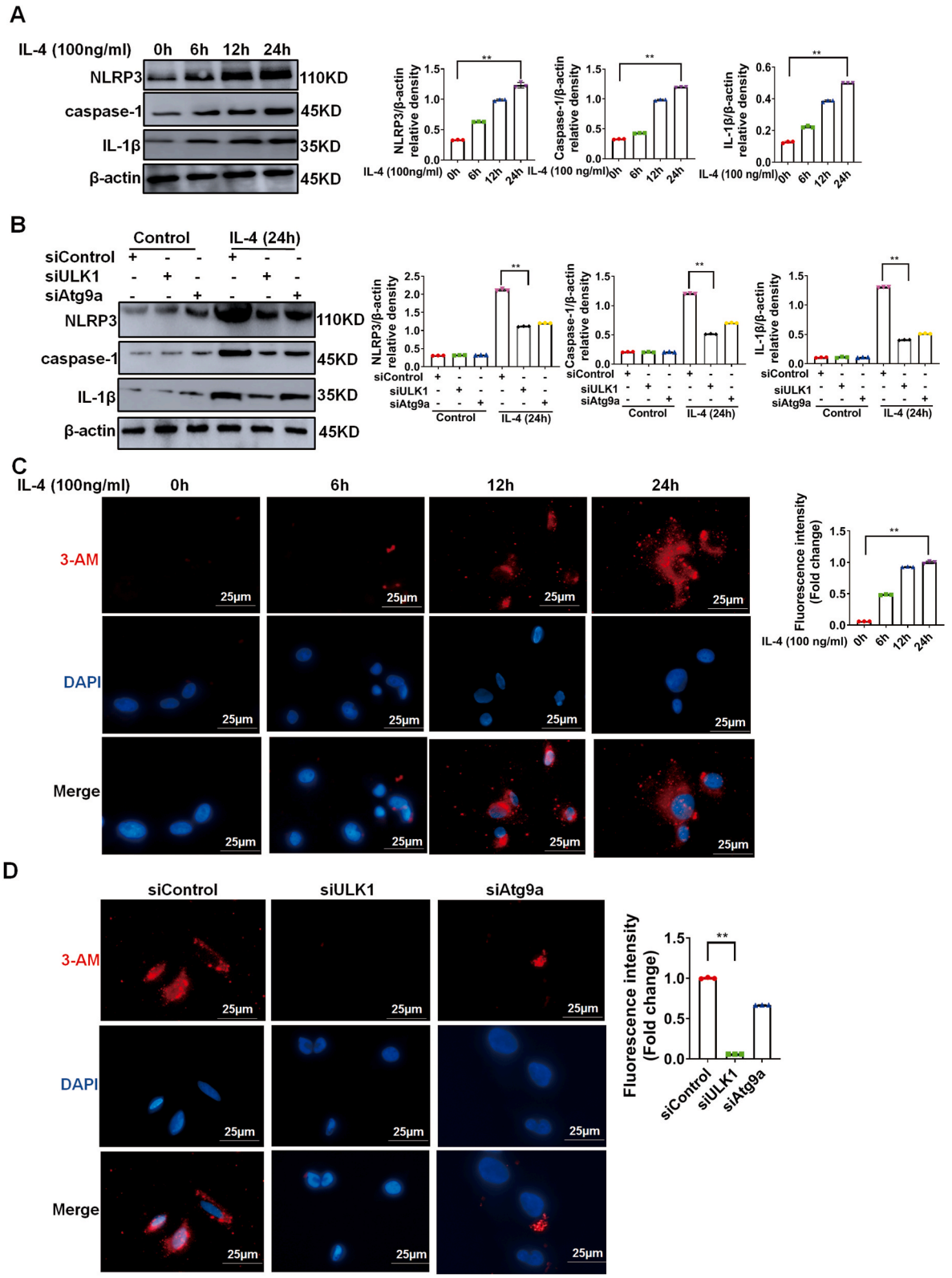

Fig. 6. IL-4-induced NLRP3 activation depends on the ULK1/Atg9a signaling pathway.
Beas-2b cells were stimulated with IL-4 for 0 h, 6 h, 12 h, and 24 h, respectively. Then, after stimulation with IL-4 for 24 h, Beas-2b cells were transfected with siULK1 and siAtg9a. **A**. Western blotting analysis of NLRP3, caspase-1, and IL-1β after IL-4 treatment. **B**. Western blotting analysis of NLRP3, caspase-1, and IL-1β after IL-4 treatment and siRNA treatment. The original full gel blots are presented in the supplementary material. **C**. Fluo 3-AM staining was used to detect the concentration of Ca^{2+} in Beas-2b cells stimulated by IL-4 (scale: 25 μm). **D**. Fluo 3-AM staining was used to detect the concentration of Ca^{2+} in Beas-2b cells after IL-4 treatment and siRNA treatment (scale: 25 μm). $^{**}p < 0.01$.

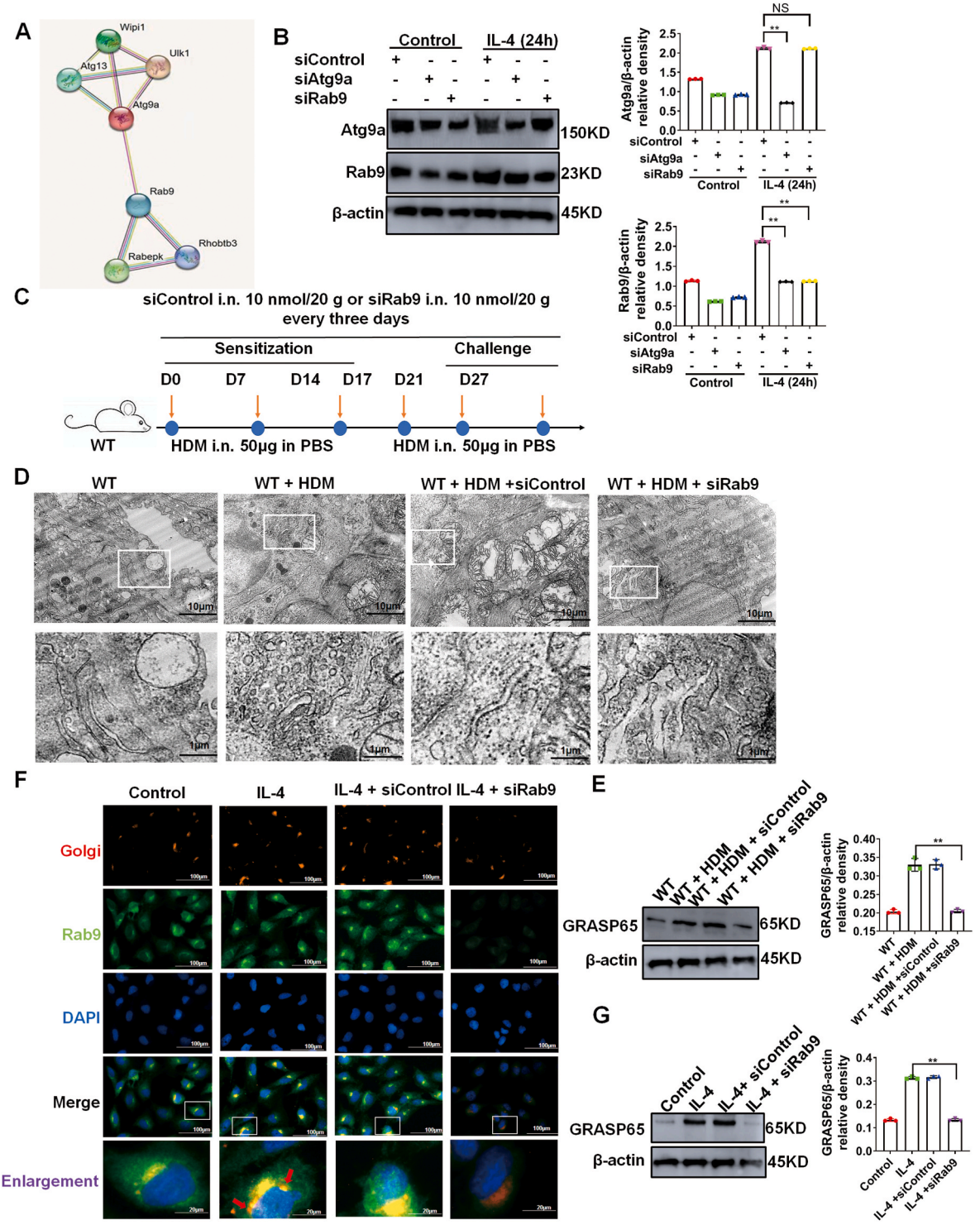

Fig. 7. Atg9a regulates the effect of Rab9 on the Golgi apparatus.
A. The protein-protein interaction network through the STRING database. **B.** Beas-2b cells were stimulated with IL-4 for 24 h and then transfected with siAtg9a and siRab9. The expression of Atg9a and Rab9 was observed through Western blotting. The original full gel blots are presented in the supplementary material. **C.** siControl and siRab9 were respectively introduced into ULK1-WT + HDM mice using nasal drip. Except WT group, mice in other groups were given 50 μg of HDM i.n. on days 0, 7, and 14, and 50 μg of HDM i.n. on days 21–27. For WT + HDM + siControl and WT + HDM + siRab9 mice, siControl and siRab9 were given i.n. every 3 days. **D.** Observation of Golgi apparatus in lung tissue using electron microscopy (scale: 10 μm). **E.** Measurement of GRASP65 expression in mouse lung tissue using Western blotting. **F.** Immunofluorescence analysis of Golgi apparatus and Rab9 expression in Beas-2b (scale: 100 μm). **G.** Measurement of GRASP65 expression in cells using Western blotting. $^{**}p < 0.01$.

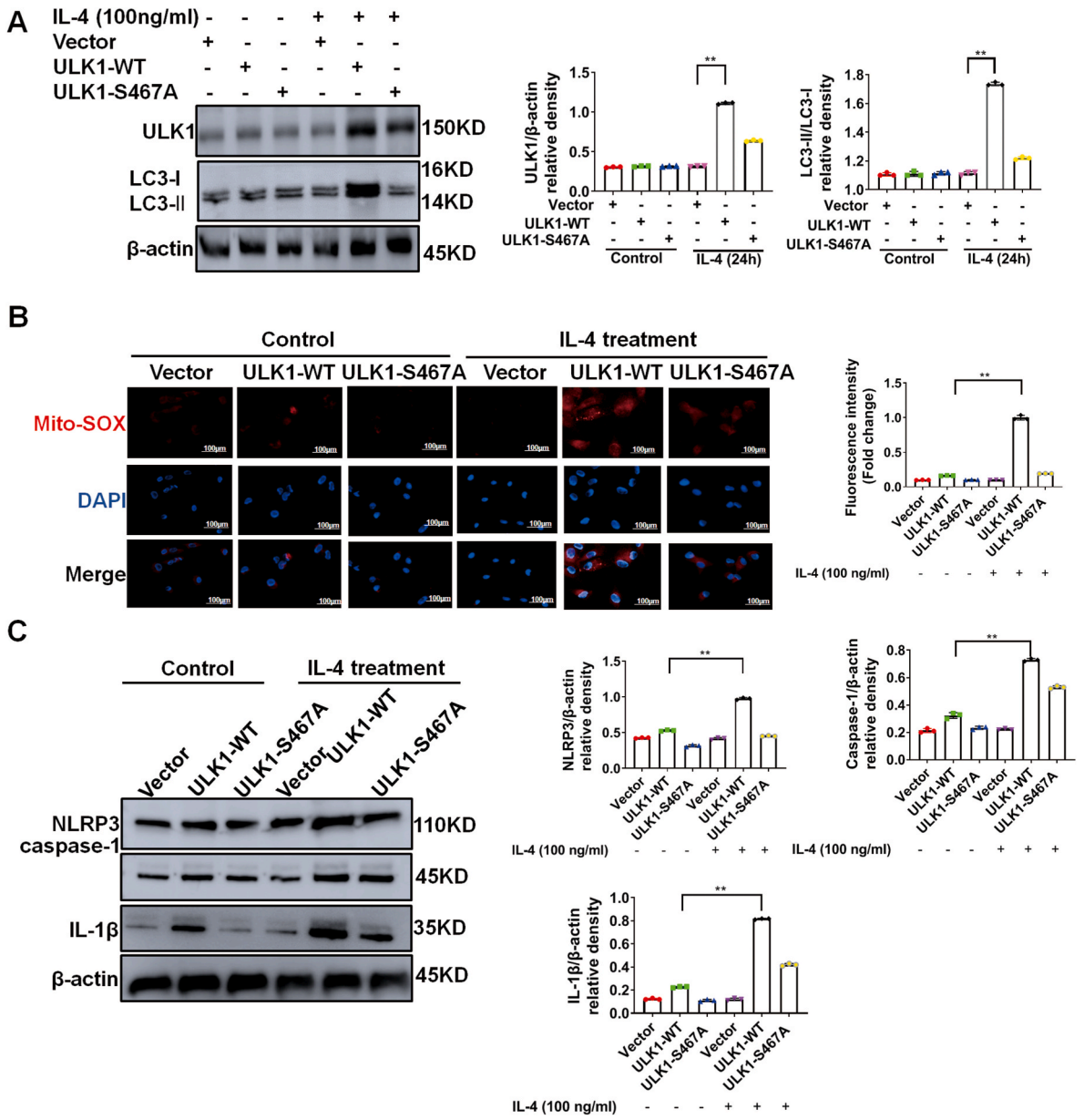

Fig. 8. The ULK1 S467 site is necessary for IL-4-induced inflammation and oxidative stress.
A. Western blotting measured the expression of ULK1 and LC3II/LC3I. **B.** Mitochondrial oxidation levels revealed by Mito-SOX expression (scale: 100 μm). **C.** Western blotting detected the expression of NLRP3, caspase-1, and IL-1β. **p < 0.01. The original full gel blots are presented in the supplementary material.

ULK1 and Atg9a were silenced in Beas-2b cells (Fig. 6D). Compared to the siControl + IL-4 group, the siULK1+IL-4 group showed a marked decrease in Ca^{2+} concentration. Therefore, it can be inferred that the ULK1/Atg9a signaling pathway is pivotal in IL-4-induced epithelial cell inflammation.

3.7. Atg9a regulates the effect of Rab9 on the Golgi apparatus

Through analysis with the STRING database, we found that Atg9a may interact with Rab9 (Fig. 7A). In addition, western blotting revealed that the siAtg9a + IL-4 group showed a significant decrease in both Atg9a and Rab9 expression compared to the siControl + IL-4 group (Fig. 7B). In contrast, in siRab9 + IL-4 group, only the Rab9 expression decreased (Fig. 7B). The results indicate that Atg9a is upstream of Rab9.

Rab9 plays a crucial role in asthma attacks and is involved in the transportation of the Golgi apparatus. To examine the effect of Rab9 on the Golgi apparatus, WT, and ULK1$^{-/-}$ mice were stimulated with HDM, respectively. Co-staining of Rab9 and the Golgi apparatus in lung tissue revealed their co-localization (Supplementary Fig. S2A). Additionally, in the WT + HDM group, there was an increase in Rab9 expression in the Golgi apparatus compared to the WT group. The expression of Rab9 in the ULK1$^{-/-}$ + HDM group was lower than that in the WT + HDM group. We also introduced siControl and siRab9 into WT + HDM mice and found that the expression of Rab9 in the lung tissue was successfully silenced by siRab9 (Supplementary Fig. S2). We found in the lung tissue of mice stimulated by HDM that the Golgi apparatus had a loose structure and extremely irregular morphology, with visible granular and fragmented Golgi apparatus (Fig. 7C and 7D). However, siRab9 inhibited the fragmentation of the Golgi apparatus caused by HDM. GRASP65 is involved in various physiological and pathophysiological processes that can alter the morphology of the Golgi apparatus, such as Golgi fragmentation. Here, western blotting found that the expression of GRASP65 was increased after HDM stimulation in WT mice, but was decreased after nasal administration of siRab9 compared to the WT +

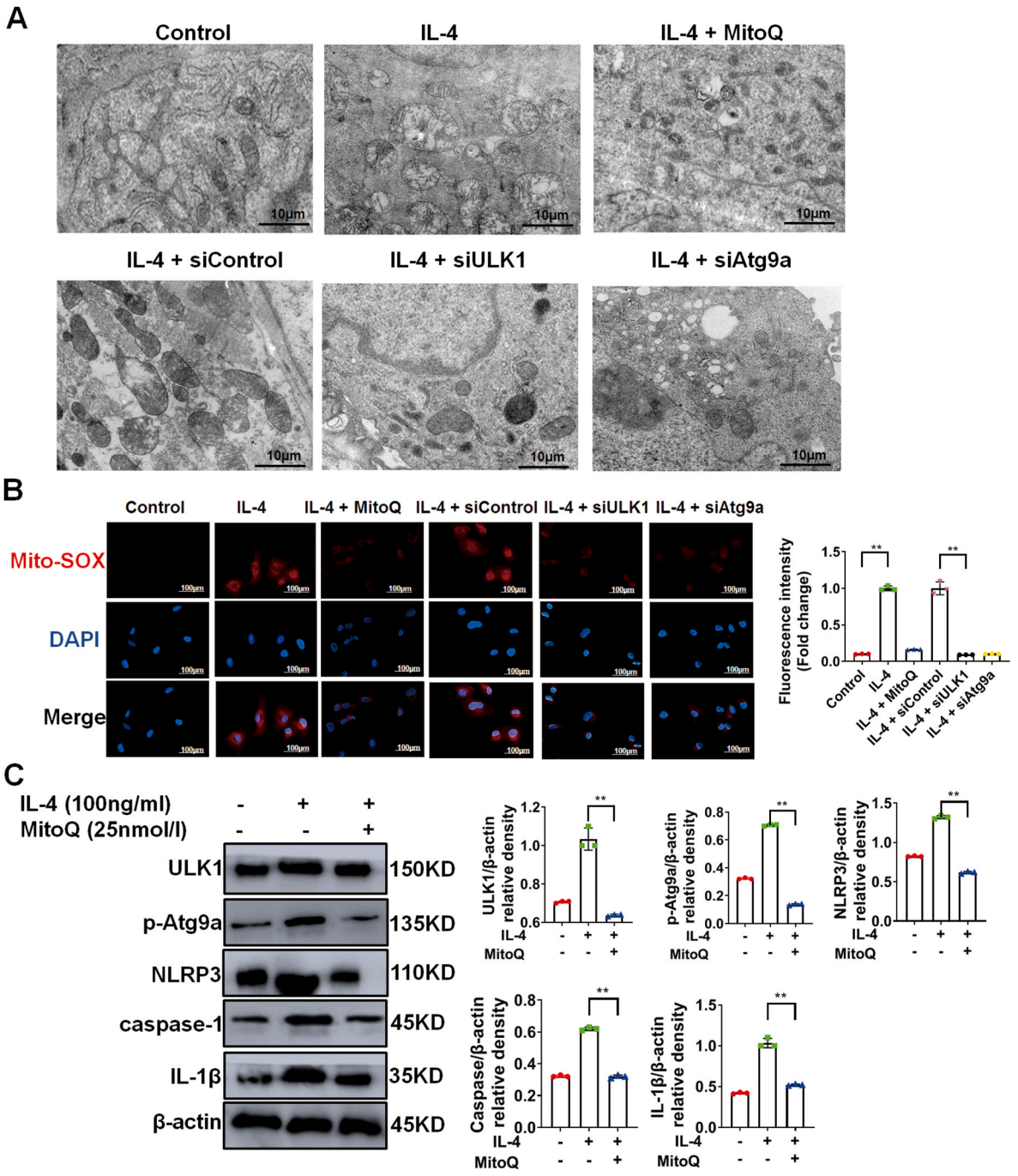

Fig. 9. Inhibition of mitochondrial oxidative stress to suppress NLRP3 inflammasome activation through the ULK1/Atg9a pathway.
Beas-2b cells were stimulated with IL-4 for 24 h. Then, after stimulation with IL-4 for 24 h, Beas-2b cells were transfected with MitoQ, siULK1 and siAtg9a. **A.** Transmission electron microscopy observation of mitochondrial changes in each group. **B.** The mitochondrial oxidation level of Beas-2b cells was evaluated with Mito-SOX staining (scale: 100 μm). **C.** Western blotting detected the expression of p-ULK1, Atg9a, NLRP3, caspase-1, and IL-1β. $^{**}p < 0.01$. The original full gel blots are presented in the supplementary material.

HDM group (Fig. 7E).

In vitro, analysis with a transmission electron microscope found that the Golgi apparatus in the IL-4-stimulated group underwent morphological lysis (Supplementary Fig. S2B). Similarly, in Beas-2b cells, Rab9 silence inhibited the inflammation-induced fragmentation of the Golgi apparatus. We stimulated Beas-2b cells with IL-4 for 24 h and found that Rab9 co-located with the Golgi apparatus in the cells (Fig. 7F). We also found that after siRab9, Rab9 was no longer expressed in the cells. In the IL-4 group, red fluorescence spread throughout the entire cytoplasm in a dot-like pattern. Finally, western blotting displayed that after IL-4 stimulation, the expression of GRASP65 increased, while decreased after siRab9 compared to the IL-4 group (Fig. 7G). These findings highlight the crucial role of Atg9a in regulating Rab9 and Rab9 in the fragmentation of the Golgi apparatus induced by inflammation.

3.8. The ULK1 S467 site is necessary for IL-4-induced inflammation and oxidative stress

To determine the significance of the ULK1 S467 site in IL-4-induced autophagy, we infected Beas-2b-ULK1-KO cells with lentivirus

containing ULK1-WT and ULK1-S467A genes. In comparison to the Vector + IL-4 group, IL-4 stimulation significantly increased levels of ULK1 and LC3-II/LC3-I in the supernatant of the ULK1-WT group (Fig. 8A).

To test whether the ULK1 S467 site is a necessary condition for IL-4-induced oxidative stress, we detected Mito-SOX, TOM20, and anti-DNA by using immunofluorescence. We found that Beas-2b-ULK1-KO cells infected with ULK1-WT exhibited an upregulation of Mito-SOX expression (Fig. 8B) and downregulation of TOM20 and anti-DNA expression upon IL-4 stimulation (Supplementary Fig. S3A). However, such changes were not observed in Beas-2b-ULK1-KO cells infected with ULK1-S467A. The relative proportion of JC-1 aggregates to JC-1 monomers is commonly used to assess mitochondrial depolarization. The decrease of mitochondrial membrane potential is a marker event of early apoptosis. Notably, we observed a notable reduction in the mitochondrial membrane potential in the ULK1-WT + IL-4 group compared to the ULK1-WT group (Supplementary Fig. S3B). Upon IL-4 stimulation, Beas-2b-ULK1-KO cells infected with ULK1-WT showed upregulation of NLRP3, caspase-1, and IL-1β expression (Fig. 8C). Therefore, ULK1-S467 is essential for IL-4-induced inflammation. Collectively, these results indicate that the ULK1 S467 site is necessary for IL-4-induced inflammation and oxidative stress.

3.9. Inhibition of mitochondrial oxidative stress to suppress NLRP3 inflammasome activation through the ULK1/Atg9a pathway

MitoQ functions as a mitochondrial-targeted antioxidant. Transmission electron microscopy observed an increase in the number of mitochondria in the IL-4 group. The outer membrane exhibits damage with minimal swelling density. Vacuolarization and mitochondrial cristae were not visible. Treatment with MitoQ, siULK1, and siAtg9a resulted in a decrease in mitochondrial damage in IL-4-stimulated Beas-2b cells (Fig. 9A).

After IL-4 stimulation, the expression level of Mito SOX increased significantly. Compared with the siControl group, the siULK1 group showed the greatest decrease in Mito SOX expression (Fig. 9B). Therefore, siULK1 can reduce the reactivity of mitochondria to ROS. As shown in Supplementary Fig. 4A, JC-1 staining showed that the potential of the mitochondrial membrane decreased. However, the mitochondrial membrane potential increased significantly in the siULK1 group than in the siControl group. Moreover, TOM20 and mtDNA dramatically decreased at 24 h after IL-4 stimulation (Supplementary Fig. 4B). Nevertheless, the siULK1 group had the most significant increase in TOM20 and mtDNA expression when compared to the siControl group. After IL-4 stimulation, under the action of MitoQ, the ULK1, p-Atg9a, and NLRP3 activation decreased (Fig. 9C). These results indicate that NLRP3 inflammasome activation can be inhibited by suppressing mitochondrial oxidative stress through the ULK1/Atg9a pathway.

4. Discussion

One of the primary causes of asthma development is persistent airway inflammation. T cells are crucial regulators of the asthmatic inflammatory process [27]. In our study, we found that deletion of the ULK1 gene reduced inflammatory cell infiltration, goblet cell proliferation, and BALF inflammatory cell infiltration, and restored the Th1/Th2 imbalance in mice with HDM-induced asthma. This gene deletion also prevented the activation of NLRP3 inflammasomes, consequently reducing the inflammatory response associated with HDM-induced asthma. Although the importance of NLRP3 inflammasomes in asthma is well-established, the underlying mechanisms remain unknown. Our *in vivo* tests revealed that the ULK1 agonist promoted inflammasome production in HDM-induced asthmatic mice. Nevertheless, ULK1 inhibitors effectively prevented the production of inflammasomes in asthmatic mice induced by HDM. These findings indicate that the ULK1 a critical factor in inflammasome formation, plays a decisive role in regulating HDM-induced asthma in mice.

We observed co-expression of ULK1 and Atg9a in mouse lung epithelial cells and lung tissue. However, the expression of Atg9a was found to be lower in the lung tissue of ULK1 gene knockout mice. Through *in vitro* and *in vivo* experiments, we found that Atg9a may serve as a secondary signaling pathway for ULK1. It is worth noting that pulmonary bronchial epithelial cells exhibited stronger expression of ULK1 and Atg9a compared to alveoli. In the context of allergic asthma, IL-4 plays a pivotal role as an effector cytokine of Th2 cells and is indispensable for inducing inflammation in B cells both *in vitro* and *in vivo* [28,29]. Our Co-IP data demonstrated the interaction between ULK1 (at the Ser 467 site) and Atg9a. The activation of the ULK1/Atg9a pathway in epithelial cells is dependent on the critical role of the ULK1 Ser 467 in response to IL-4. ULK1 Ser 467 regulates mitochondrial homeostasis during starvation [30]. Therefore, we hypothesize that IL-4 stimulation for 24 h activates the ULK1/Atg9a pathway (specifically at Ser 467 of ULK1), leading to the release of cellular inflammatory components and the generation of ROS, ultimately exacerbating asthma. The site of ULK1 at Ser 467 plays a significant role in mitosis [30,31]. Here, we established stable cell lines by infecting Beas-2b-ULK1-KO cells with lentivirus carrying ULK1-WT and ULK1-S467A genes. After stimulation with IL-4, it was found that the ULK1-S467A gene resulted in reduced inflammation compared to the ULK1-WT gene, indicating that the site of ULK1 at S467 is a crucial factor in IL-4-induced inflammation. Additionally, analysis of indicators of cellular oxidative stress revealed that the site of ULK1 at S467 was essential for IL-4-induced oxidative stress. Moreover, we found through *in vitro* experiments that ULK1 phosphorylated Atg9a at S14.

We observed a close association between ULK1 and Atg9a, as well as between Atg9a and Rab9, on the STRING database. It has been reported that under high-temperature stress, ubiquitinated ATG9A was involved in regulating dynamic Golgi apparatus changes, enhancing the comprehension of its novel role in non-classical autophagy [33]. Therefore, we speculate whether there is also an interaction between ULK1 and Rab9. Moreover, we also speculate whether Rab9 is involved in changes in the Golgi body. Additionally, our *in vitro* studies suggested that Rab9 may serve as a secondary signaling pathway for Atg9a. NLRP3, which is activated during inflammation, accumulates around various vesicle structures, forming polymers [34], which are derived from the disrupted Golgi apparatus network [35]. Interestingly, we observed a novel phenomenon that inflammatory stimulation could lead to fragmentation of the Golgi apparatus in asthma. Silencing Rab9 significantly inhibited the inflammation-induced fragmentation of the Golgi apparatus. This supports our belief in the crucial role of Rab9 in Golgi fragmentation.

IL-4 can regulate the differentiation of $CD4^+$ T cells into Th2 cells. Despite the importance of IL-4 in asthma, its role in asthma regulation has not been fully elucidated. Our *in vitro* experiments revealed that IL-4 induced the formation of inflammatory bodies in epithelial cells, and this process relied on the ULK1/Atg9a signaling pathway. Additionally, it has been shown that the calcium ion channel [32] plays a significant role in chronic airway inflammation, airway hyperresponsiveness, and airway remodeling. Through Fluo 3-AM immunofluorescence, we demonstrated the necessity of the ULK1/Atg9a/Rab9 signaling pathway in mediating the IL-4-induced increase in Ca^{2+} concentration in epithelial cells. ULK1 knockout alleviates mitochondrial oxidative stress in epithelial cells stimulated by inflammation. Immunofluorescence analysis using DHE showed that HDM stimulation had no evident impact on ROS in $ULK1^{-/-}$ mice. In this study, cell experiments showed that IL-4 induced mitochondrial oxidative stress in epithelial cells through the ULK1/Atg9a signaling pathway. We then monitored the changes in mitochondrial membrane potential in lung epithelial cells and found that blocking the ULK1/Atg9a signaling pathway increased the mitochondrial potential following IL-4 stimulation. The TOM20 complex, a mitochondrial marker, is located on the outer membrane of mitochondria. Mitochondria-derived ROS have the potential to damage proteins,

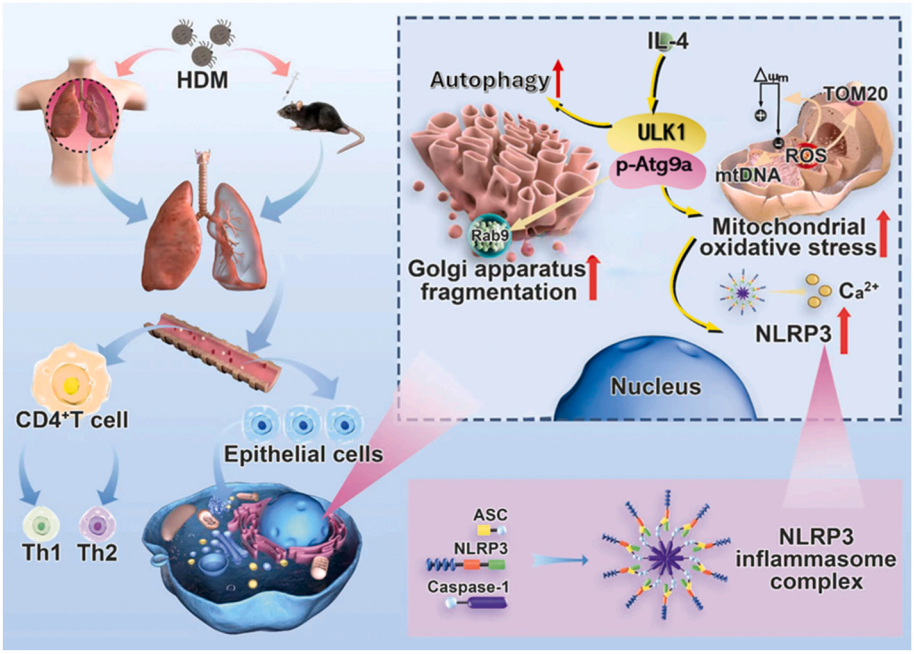

Fig. 10. Schematic diagram illustrating the occurrence of asthma.
HDM causes TH1/TH2 response imbalance by affecting lung tissue in humans and mice. IL-4 stimulates epithelial cells and triggers the ULK1/Atg9a/Rab9 signaling pathway, leading to increased inflammation and oxidative stress within these cells, and Golgi apparatus division.

membranes, and mtDNA within the cell [33]. Our results indicate that blocking the ULK1/Atg9a signaling pathway may alleviate oxidative-induced mitochondrial damage, suggesting that this signaling pathway may play a role in reducing ROS-induced mitochondrial damage.

This study has some limitations. For example, the sample size was relatively small. Moreover, we did not further examine how epithelial cell inflammation impacts the smooth muscle cells below with regard to bronchodilation. Further studies are warranted.

5. Conclusions

Overall, we revealed here for the first time that the ULK1/Atg9a/Rab9 signaling pathway was involved in HDM-induced asthma and played a crucial role in the Golgi apparatus, the inflammatory and oxidative stress processes associated with asthma (Fig. 10). Moreover, Atg9a could interact with ULK1 at Ser467, and Atg9a and ULK1 co-localized in the epithelial cells. ULK1 phosphorylated Atg9a at Ser14. Rab9 greatly contributed to the fragmentation of the Golgi apparatus induced by inflammation. Furthermore, the ULK1/Atg9a pathway may also activate inflammasomes through mitochondrial oxidative stress, thereby promoting inflammation of the lung epithelium. These findings may provide potential new therapeutic targets for asthma treatment.

Funding

This work was supported by the National Natural Science Foundation of China (Grant numbers: 81970018, 82160004, 82060008 and 82260007). The funder had no role in the study.

CRediT authorship contribution statement

Chang Xu: Writing – review & editing, Writing – original draft, Software, Methodology, Investigation, Funding acquisition, Formal analysis, Data curation. **Yilan Song:** Writing – review & editing, Writing – original draft, Software, Methodology, Investigation, Funding acquisition, Formal analysis, Data curation. **Wanting Liu:** Writing – review & editing, Investigation, Formal analysis, Data curation. **Ruobai Liu:** Writing – review & editing, Investigation, Formal analysis, Data curation. **Qiaoyun Bai:** Writing – review & editing, Investigation, Formal analysis, Data curation. **Liangchang Li:** Writing – review & editing, Methodology, Investigation, Formal analysis. **Chongyang Wang:** Writing – review & editing, Funding acquisition, Data curation, Conceptualization. **Guanghai Yan:** Writing – review & editing, Validation, Project administration, Funding acquisition, Data curation, Conceptualization.

Declaration of competing interest

The authors declare that they have no known competing financial interests or personal relationships that could have appeared to influence the work reported in this paper.

Data availability

Data will be made available on request.

Acknowledgments

Not applicable.

Appendix A. Supplementary data

Supplementary data to this article can be found online at https://doi.org/10.1016/j.redox.2024.103090.

References

[1] M.I. Asher, L. Garcia-Marcos, N.E. Pearce, D.P. Strachan, Trends in worldwide asthma prevalence, Eur. Respir. J. 56 (6) (2020).
[2] W. Luo, J. Hu, W. Xu, J. Dong, Distinct spatial and temporal roles for Th1, Th2, and Th17 cells in asthma, Front. Immunol. 13 (2022) 974066.
[3] A. Gallagher, M. Edwards, P. Nair, S. Drew, A. Vyas, R. Sharma, P.A. Marsden, R. Wang, D.J. Evans, Anti-interleukin-13 and anti-interleukin-4 agents versus placebo, anti-interleukin-5 or anti-immunoglobulin-E agents, for people with asthma, Cochrane Database Syst. Rev. 10 (10) (2021). CD012929.

[4] Y. Xu, W. Wan, Acetylation in the regulation of autophagy, Autophagy 19 (2) (2023) 379–387.
[5] Y. He, H. She, T. Zhang, H. Xu, L. Cheng, M. Yepes, Y. Zhao, Z. Mao, p38 MAPK inhibits autophagy and promotes microglial inflammatory responses by phosphorylating ULK1, J. Cell Biol. 217 (1) (2018) 315–328.
[6] M. Zhu, G. Deng, P. Tan, C. Xing, C. Guan, C. Jiang, Y. Zhang, B. Ning, C. Li, B. Yin, K. Chen, Y. Zhao, H.Y. Wang, B. Levine, G. Nie, R.F. Wang, Beclin 2 negatively regulates innate immune signaling and tumor development, J. Clin. Invest. 130 (10) (2020) 5349–5369.
[7] Y. Wang, Q. Chen, F. Jiao, C. Shi, M. Pei, L. Wang, Z. Gong, Histone deacetylase 2 regulates ULK1 mediated pyroptosis during acute liver failure by the K68 acetylation site, Cell Death Dis. 12 (1) (2021) 55.
[8] Y.T. Wang, T.Y. Liu, C.H. Shen, S.Y. Lin, C.C. Hung, L.C. Hsu, G.C. Chen, K48/K63-linked polyubiquitination of ATG9A by TRAF6 E3 ligase regulates oxidative stress-induced autophagy, Cell Rep. 38 (8) (2022) 110354.
[9] D. Matheoud, A. Sugiura, A. Bellemare-Pelletier, A. Laplante, C. Rondeau, M. Chemali, A. Fazel, J.J. Bergeron, L.E. Trudeau, Y. Burelle, E. Gagnon, H. M. McBride, M. Desjardins, Parkinson's disease-related proteins PINK1 and parkin repress mitochondrial antigen presentation, Cell 166 (2) (2016) 314–327.
[10] Y.G. Zhao, P. Codogno, H. Zhang, Machinery, regulation and pathophysiological implications of autophagosome maturation, Nat. Rev. Mol. Cell Biol. 22 (11) (2021) 733–750.
[11] C.W. Yang, C.D. Hojer, M. Zhou, X. Wu, A. Wuster, W.P. Lee, B.L. Yaspan, A. C. Chan, Regulation of T Cell receptor signaling by DENND1B in TH2 cells and allergic disease, Cell 164 (1–2) (2016) 141–155.
[12] D. Lombardi, T. Soldati, M.A. Riederer, Y. Goda, M. Zerial, S.R. Pfeffer, Rab9 functions in transport between late endosomes and the trans Golgi network, EMBO J. 12 (2) (1993) 677–682.
[13] Y. Bordon, Trans-Golgi network breaks away to activate NLRP3, Nat. Rev. Immunol. 19 (2) (2019) 68–69.
[14] H. Akel Bilgic, B. Kilic, B.D. Kockaya, B.E. Sarac, A. Kilic Suloglu, O. Kalayci, C. Karaaslan, Oxidative stress stimulation leads to cell-specific oxidant and antioxidant responses in airway resident and inflammatory cells, Life Sci. 315 (2023) 121358.
[15] J.M. Suski, M. Lebiedzinska, M. Bonora, P. Pinton, J. Duszynski, M.R. Wieckowski, Relation between mitochondrial membrane potential and ROS formation, Methods Mol. Biol. 810 (2012) 183–205.
[16] F. Hou, J. Huang, F. Qing, T. Guo, S. Ouyang, L. Xie, Y. Ding, J. Yu, Y. Li, X. Liu, T. S. He, X. Fan, Z. Liu, The rare-earth yttrium induces cell apoptosis and autophagy in the male reproductive system through ROS-Ca(2+)-CamkII/Ampk axis, Ecotoxicol. Environ. Saf. 263 (2023) 115262.
[17] X. Sun, W. Zhang, Y. Wang, Y. Zhang, X. Liu, X. Shi, S. Xu, Combined exposure to di (2-ethylhexyl) phthalate and polystyrene microplastics induced renal autophagy through the ROS/AMPK/ULK1 pathway, Food Chem. Toxicol. : Int. J. Pub. British Indus. Biol. Res. Assoc. 171 (2023) 113521.
[18] Y.T. Wang, G.C. Chen, Regulation of oxidative stress-induced autophagy by ATG9A ubiquitination, Autophagy 18 (8) (2022) 2008–2010.
[19] E. Theofani, M. Semitekolou, K. Samitas, A. Mais, I.E. Galani, V. Triantafyllia, J. Lama, I. Morianos, A. Stavropoulos, S.J. Jeong, E. Andreakos, B. Razani, N. Rovina, G. Xanthou, TFEB signaling attenuates NLRP3-driven inflammatory responses in severe asthma, Allergy 77 (7) (2022) 2131–2146.
[20] G. Deng, C. Li, L. Chen, C. Xing, C. Fu, C. Qian, X. Liu, H.Y. Wang, M. Zhu, R. F. Wang, BECN2 (beclin 2) negatively regulates inflammasome sensors through atg9a-dependent but ATG16L1- and LC3-independent non-canonical autophagy, Autophagy 18 (2) (2022) 340–356.
[21] V. Mishra, J. Banga, P. Silveyra, Oxidative stress and cellular pathways of asthma and inflammation: therapeutic strategies and pharmacological targets, Pharmacol. Therapeut. 181 (2018) 169–182.
[22] G.E. Carpagnano, G. Scioscia, D. Lacedonia, P. Soccio, C.M.I. Quarato, G. Cotugno, M.G. Palumbo, M.P. Foschino Barbaro, Searching for inflammatory and oxidative stress markers capable of clustering severe asthma, Arch. Bronconeumol. 57 (5) (2021) 338–344.
[23] Y.A. Mebratu, K.R. Smith, G.E. Agga, Y. Tesfaigzi, Inflammation and emphysema in cigarette smoke-exposed mice when instilled with poly (I:C) or infected with influenza A or respiratory syncytial viruses, Respir. Res. 17 (1) (2016) 75.
[24] C.R. Crowe, K. Chen, D.A. Pociask, J.F. Alcorn, C. Krivich, R.I. Enelow, T.M. Ross, J.L. Witztum, J.K. Kolls, Critical role of IL-17RA in immunopathology of influenza infection, J. Immunol. 183 (8) (2009) 5301–5310.
[25] L. Zhang, L. Fu, S. Zhang, J. Zhang, Y. Zhao, Y. Zheng, G. He, S. Yang, L. Ouyang, B. Liu, Discovery of a small molecule targeting ULK1-modulated cell death of triple negative breast cancer in vitro and in vivo, Chem. Sci. 8 (4) (2017) 2687–2701.
[26] K.R. Martin, S.L. Celano, A.R. Solitro, H. Gunaydin, M. Scott, R.C. O'Hagan, S. D. Shumway, P. Fuller, J.P. MacKeigan, A potent and selective ULK1 inhibitor suppresses autophagy and sensitizes cancer cells to nutrient stress, iScience 8 (2018) 74–84.
[27] R. He, S. Wang, S. Yang, R. Liu, N. Nan, X. Lu, M. Gong, J. Li, Shaoyao-Gancao-Tang regulates the T-helper-type 1/T-helper-type 2 ratio in the lung and gut and alters gut microbiota in rats with ovalbumin-induced asthma, J. Ethnopharmacol. 309 (2023) 116300.
[28] C. Pelaia, E. Heffler, C. Crimi, A. Maglio, A. Vatrella, G. Pelaia, G.W. Canonica, Interleukins 4 and 13 in asthma: key pathophysiologic cytokines and druggable molecular targets, Front. Pharmacol. 13 (2022) 851940.
[29] F. Xia, C. Deng, Y. Jiang, Y. Qu, J. Deng, Z. Cai, Y. Ding, Z. Guo, J. Wang, IL4 (interleukin 4) induces autophagy in B cells leading to exacerbated asthma, Autophagy 14 (3) (2018) 450–464.
[30] N. Dephoure, C. Zhou, J. Villen, S.A. Beausoleil, C.E. Bakalarski, S.J. Elledge, S. P. Gygi, A quantitative atlas of mitotic phosphorylation, Proc. Natl. Acad. Sci. U.S. A. 105 (31) (2008) 10762–10767.
[31] C. Lin, A.M. Blessing, T.L. Pulliam, Y. Shi, S.R. Wilkenfeld, J.J. Han, M.M. Murray, A.H. Pham, K. Duong, S.N. Brun, R.J. Shaw, M.M. Ittmann, D.E. Frigo, Inhibition of CAMKK2 impairs autophagy and castration-resistant prostate cancer via suppression of AMPK-ULK1 signaling, Oncogene 40 (9) (2021) 1690–1705.
[32] Y. Lai, G. Fois, J.R. Flores, M.J. Tuvim, Q. Zhou, K. Yang, J. Leitz, J. Peters, Y. Zhang, R.A. Pfuetzner, L. Esquivies, P. Jones, M. Frick, B.F. Dickey, A. T. Brunger, Inhibition of calcium-triggered secretion by hydrocarbon-stapled peptides, Nature 603 (7903) (2022) 949–956.
[33] C. Michaeloudes, H. Abubakar-Waziri, R. Lakhdar, K. Raby, P. Dixey, I.M. Adcock, S. Mumby, P.K. Bhavsar, K.F. Chung, Molecular mechanisms of oxidative stress in asthma, Mol. Aspect. Med. 85 (2022) 101026.